Wavelength Dependence of a Vertically Coupled Resonator-Waveguide System

Fabio Turri, Fernando Ramiro-Manzano, Iacopo Carusotto, Mher Ghulinyan, Georg Pucker, and Lorenzo Pavesi, *Senior Member, IEEE*

***Abstract*—Coupling of light to and from a microdisk resonator is a crucial step for the integration of this photonic structure in a photonic integrated circuit. However, the most common lateral coupling scheme, based on a point contact with a coplanar bus waveguide, suffers from strong wavelength dependence. This is a limiting factor for exciting efficiently the resonant modes in a broad spectral region. In the present paper, we propose a solution based on a different configuration, known as vertical coupling configuration, where a bus waveguide is buried below the micro disk. We demonstrate theoretically and experimentally that the long interaction region provided by this geometry allows to extend the optimal coupling spectral range from *IR* to visible. This feature constitutes a remarkable advantage over the usual laterally coupled devices for many different applications, such as frequency conversion, allowing bandwidth limitations to be significantly diminished.**

***Index Terms*—All-optical devices, integrated optics devices, microcavity devices, resonators.**

I. Introduction

WHISPERING Gallery Mode resonators (WGMr) are becoming fundamental building blocks for the manipulation of optical signals in integrated photonic devices [1]. The enhanced optical power circulating into the cavity, described by the Quality-factor (Q), produces several interesting effects such as lasing [2] and enhances drastically other phenomena such as optomechanical interaction and nonlinear processes [3], [4]. For probing experimentally a resonator, a coupling technique based on the interaction of the evanescent field of a signal propagating in a tapered optical fiber and of the WGM of the resonator is commonly adopted [5], [6]. However, for a practical application of a WGMr in a photonic chip, the integration of both the cavity and the interrogating element is crucial [7]. As a result, a bus waveguide fabricated within the same layer and with the same lithographic process of the WGMr is the common solution [8]. This lateral coupling geometry is based on the overlap between the modes of the two structures (resonator and waveguide) and it is critically dependent on the gap distance between them [9], [10]. Moreover, these side coupled integrated devices intrinsically suffer from bandwidth limitations because of the monotonic dependence of the modes overlap with respect to wavelength. Several efforts have been made to create an integrated structure with a wavelength-independent behavior. In particular, T. Carmon *et al.* [11] proposed to bend the bus element. Coupling was achieved at extreme wavelengths of 682 and 1540 nm, albeit with a difference of about 50% in the transmission.

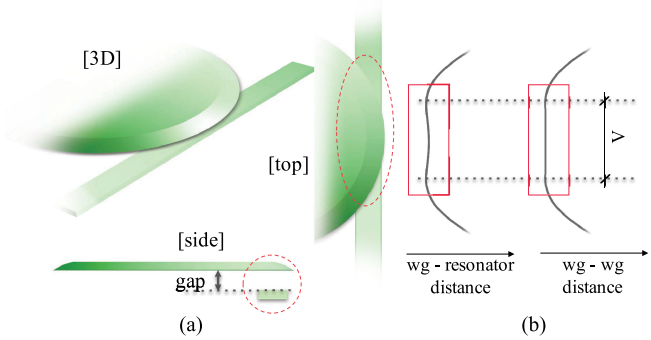

Fig. 1. (a) schematic representation of the microdisk-bus waveguide system with the coupling region highlighted by red circles; (b) effective distance between the two coupling elements in a vertically coupled system (left) compared to the distance between waveguides in a directional coupler (right).

To widen the working wavelength range we propose an alternative route based on a vertically coupled scheme [12]. In such a device, the interaction between the two elements should not be considered to take place in a single point anymore. Indeed, the placement of the bus waveguide under the resonator enlarges the area of interaction as depicted in Fig. 1(a). In particular, it comes out from geometrical considerations that the distance between the guided modes of the two elements is kept almost constant over a wide area (see Fig. 1(b)), called flat zone (Λ), which can be considered as the effective interaction region of the system [13]. The existence of this flat zone makes the system very similar to a directional coupler and suggests to adopt this structure as an approximation of the vertically coupled device. Moreover, the flat zone presents a dependence on the vertical gap distance (L_v) between the waveguide and the resonator. As a result, the coupling coefficient, and thus the transmission and Q, depends on L_v showing a peculiar oscillatory behavior [13]. In this work, we extend this peculiarity of the vertical coupling scheme to the wavelength dependence of the coupling coefficient.

Indeed, the Coupled Mode Theory (CMT) applied to directional couplers shows that coupling of light from one waveguide

Manuscript received July 15, 2016; revised September 13, 2016; accepted October 2, 2016. Date of publication October 4, 2016; date of current version November 1, 2016. This work was supported by the Provincia Autonoma di Trento under ProjectSIQURO.

F. Turri, F. Ramiro-Manzano, and L. Pavesi are with the Nanoscience Laboratory, Department of Physics, University of Trento, Povo 38123, Italy (e-mail: fabio.turri@unitn.it; ferraman@science.unitn.it; lorenzo.pavesi@unitn.it).

I. Carusotto is with INO-CNR BEC Center and Department of Physics, University of Trento, Povo 38123, Italy (e-mail: iacopo.carusotto@unitn.it).

M. Ghulinyan and G. Pucker are with the Centre for Materials and Microsystems, Fondazione Bruno Kessler, Povo 38123, Italy (e-mail: ghulinyan@fbk.eu; pucker@fbk.eu).

Color versions of one or more of the figures in this paper are available online at http://ieeexplore.ieee.org.

Digital Object Identifier 10.1109/JLT.2016.2615331

to the other depends on wavelength with a periodic behavior [14] and light can be completely transferred from one waveguide to the other at different wavelengths. Therefore, in a directional coupler, and similarly in a vertically coupled system, the same coupling factor can be achieved at several wavelengths generating several critical coupling scenarios.

II. Model of the Wavelength Dependent Coupling

To verify the qualitative concept discussed in the introduction for the vertically coupled structure we here extend the model proposed in [13] to wavelength variations. In particular we start from the description of the transmittance $T(\lambda)$ in the vicinity of a resonance with a Lorentzian function:

$$T(\lambda) = \left| |A| + i \frac{\frac{c}{n_{\text{eff}1} L} B e^{-\alpha L}}{\left(\frac{2\pi c}{\lambda} - \frac{2\pi c}{\lambda_0}\right) - i\,\Gamma/2} \right|^2 \tag{1}$$

where λ_0 is the resonance wavelength and the other quantities are:

$$A = \exp\left(i\,\frac{\Delta\beta}{2}\Lambda\right)\left[\cos(\gamma\Lambda) - i\frac{\Delta\beta}{2\gamma}\sin(\gamma\Lambda)\right] \tag{2}$$

$$B = \left[\frac{C_{12}\,C_{21}}{\gamma^2}\right]\,\sin^2(\gamma\Lambda) \tag{3}$$

$$\Gamma = \frac{2c}{n_{\text{eff}1} L}\left(1 - |A| e^{-\alpha L}\right) \tag{4}$$

with:

$$\gamma = \left[(\Delta\beta)^2 + C_{12}\,C_{21}\right]^{1/2} \tag{5}$$

The parameters that appear in Eq. (2)–(5) are: c the light speed in vacuum, $n_{\text{eff}1}$ the effective index of the resonator mode, L the length of the resonator, α its intrinsic loss, Λ the flat zone length, $\Delta\beta = \beta_1 - \beta_2$ the propagation constant mismatch between the resonator and the waveguide and C_{12}, C_{21} the mode overlap coefficients.

Since we are interested in the transmission minimum $T_m(\lambda)$ (i.e. $\lambda = \lambda_0$) Eq. (1) becomes:

$$T_m(\lambda) = \left| |A| - \frac{\frac{c}{n_{\text{eff}1} L} B e^{-\alpha L}}{\Gamma/2} \right|^2 \tag{6}$$

where dependence on wavelength of the different quantities is now considered.

In analogy with the directional coupler, we describe the system by two slab waveguides. As a consequence, the explicit dependence of the different quantities on wavelength can be described by only few parameters: the geometrical parameters of the system (waveguide thickness, width and separation), the refractive indexes of the materials, the resonator effective mode radius r and its attenuation coefficient α. Indeed, the approximation allows to derive all the other quantities from analytical calculations.

From ellipsometric measurements the refractive index of the three materials constituting the system (resonator n_1, bus waveguide n_2 and cladding n_c) can be found at varying wavelengths. Then, the first waveguide mode can be obtained by solving the transcendental equation [15]:

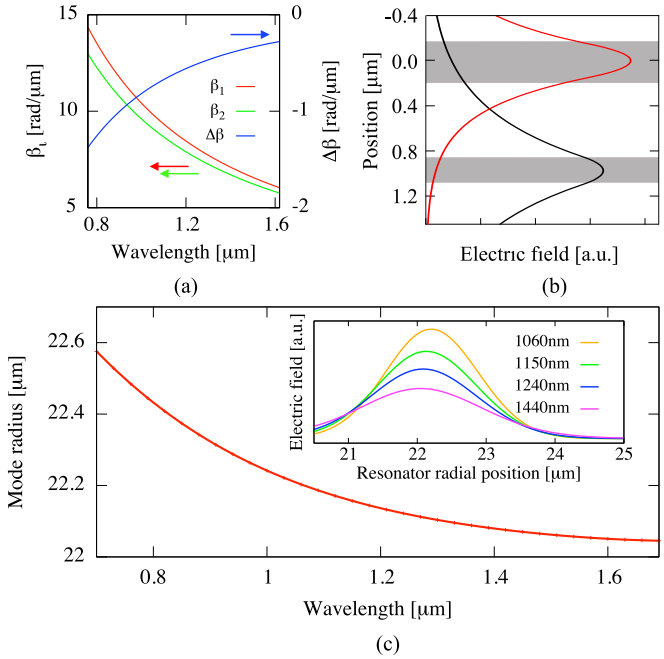

Fig. 2. (a) Propagation constants and propagation constant mismatch in the IR domain from (8); (b) normalized mode profiles calculated for the two waveguides at fixed wavelength (1.55 μm); the shaded areas defines the actual position of the two elements; (c) the radial position of the maximum of the electric field and (inset) radial shape of the mode inside the resonator at different wavelengths.

$$\tan\left(\frac{\pi\ d\ \sin(\theta_i)}{\lambda}\right) = \sqrt{\left(\frac{\sin(\frac{\pi}{2} - \theta_c)}{\sin(\theta_i)}\right)^2 - 1} \tag{7}$$

where d is the thickness of the considered waveguide, θ_i is the propagation angle, $\theta_c = n_c/n_i$ and $n_i = n_1$ or n_2 depending on whether the resonator or the bus waveguide is considered. From the angle θ_i the propagation constant and the extinction coefficient of the optical mode outside the waveguide are obtained as:

$$\beta_i = n_i\left(\frac{2\pi}{\lambda}\right)\cos(\theta_i); \quad \tau_i = n_c\frac{2\pi}{\lambda}\sqrt{\frac{\cos(\theta_i)^2}{\cos(\pi/2 - \theta_c)^2} - 1} \tag{8}$$

Therefore the propagation constant mismatch $\Delta\beta = \beta_2 - \beta_1$ can be calculated (Fig. 2(a)). With τ and β known for both the waveguides, the mode profiles along the coupling direction can be found (Fig. 2(b)) and the overlap coefficients C_{12}, C_{21} can be extrapolated from the overlap of the two fields inside the waveguides [15].

The effective index n_{eff} comes out directly from the propagation constants as $n_{\text{eff}} = \beta(2\pi/\lambda)$.

The length of the resonator is $L = 2\pi r$ with r the resonator radius, while the size of the flat zone Λ depends on the vertical distance between the waveguide and the resonator L_v, labeled gap in Fig. 1(a). Since in our experiment we are using wedge resonators (see Section 3 [16]), particular care should be paid to the different radial modes. Indeed, a univocal definition of the resonator radius is not possible due to the fact that the different

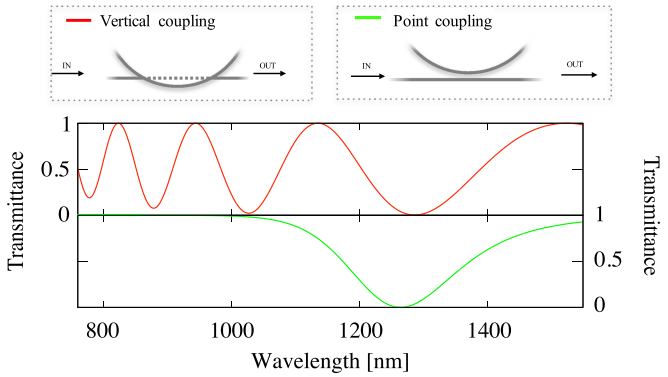

Fig. 3. Bus waveguide coupling scheme (top) and transmittance minimum dependence on wavelength(bottom) for a vertically coupled resonator as resulting from Eq. (6) and for a point coupled resonator; SiN and SiON waveguides have been considered in all the simulations, with 20 μm flat zone length in the vertical coupling case.

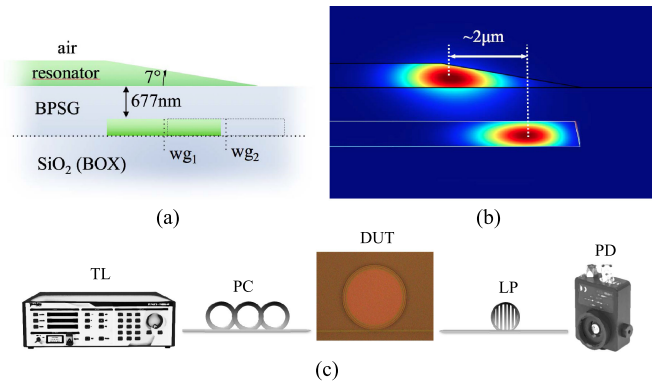

Fig. 4. (a) sketch of the device (cross-section); vertical dashed lines show the central position of the waveguide in the two configurations; (b) simulated 1^{st} order radial mode cross section for wet (top) and dry (bottom) etched disk resonators showing 2 μm difference in the mode radial position; 24 μm external radius and $\lambda = 1.55$ μm have been considered in the simulation; (c) experimental set-up for the optical characterization of the device: IR or visible light from two different tunable laser (TL) is sent in the polarization controller stage (PC) and coupled into the sample through tapered fibers; tapered fiber and polarization controller are also used to extract transmitted signal from the sample and to send it to the photodetector (PD).

modes circulate on different circumferences. As a result the parameter r represents an effective radius, which describes where the field inside the resonator reaches its maximum intensity (Fig. 2(c)), and it can be easily extrapolated from 2D finite element simulation. From this assumption the L value is directly obtained and also Λ can be derived once the relative positions of the microresonator and the bus waveguide are given. The last unknown quantity needed for the computation of Eq. (6) is the intrinsic loss of the resonator, which can be obtained from Finite Element Method (FEM) simulations.

Inserting the values for the different parameters in Eq. (6) the dependence of the transmittance on wavelength for a vertically coupled structure is obtained. An example of this is shown in Fig. 3 together with the transmittance minimum coming from a laterally coupled device [9]. In particular, in the vertical coupling geometry there are multiple critical coupling wavelengths ($T_{\min} \sim 0$). This contrasts to what is observed for a point coupling geometry, i.e. for a lateral coupling configuration, where the critical condition occurs for a single wavelength only.

III. Device Description and Optical Measurements

In order to verify the model described above we performed some measurements on a real system composed by a 350 nm-thick and 24 μm-radius SiN wedge disk resonator vertically coupled to a 250 nm-thick and 2.5 μm-wide SiON bus waveguide (Fig. 4(a)) [16]. A 7° of wedge angle is obtained by isotropic wet etching. Complete characterization of the resonator dimensions and shape has been carried out through Atomic Force Microscope (AFM) measurements described elsewhere [17]. As a consequence of the wedge geometry the optical mode radius is retracted from the external rim with respect to the one of an anisotropic dry-etched disk-resonator (Fig. 4(b)). The extent of retraction depends on the considered wavelength (see Fig. 2(c)) and on the observed optical mode [16]. The resonator vertical position is fixed 677 nm above the waveguide with BoroPhosphoSilicate Glass (BPSG) cladding placed in between. Fig. 4(a) shows the two possible configurations corresponding to horizontal distances of 2 or 1 μm between the centre of the waveguide and the outer rim of the disk. Henceforth we label these alignments wg_1 and wg_2 respectively. A 2 μm thick SiO_2 cladding layer below the waveguide allows to isolate the optical modes from the Si substrate at the bottom of the wafer. Detailed description of the fabrication process can be found elsewhere [16].

Optical measurements have been carried out in the visible and in the IR range: specifically from 760 nm to 795 nm and from 1440 nm to 1630 nm, with resolution of 3pm and 1pm respectively. A sketch of the experimental set-up is shown in Fig. 4(c). Light from a tunable laser source has been coupled in and out from the sample using tapered lensed fibers and the transmitted signal has been acquired with a Ge photodetector. A polarisation controller in the input stage and a linear polariser at the output have been inserted in order to ensure the excitation and detection of a TE mode propagating in the bus waveguide. All the experiments have been carried out at room temperature under stable and controlled conditions.

IV. Results

We first focus on the results coming from the wg_2 configuration, whose visible and IR spectra are shown in Fig. 5. Both spectra show the typical periodic peaks related to resonant guided modes, with several order family modes coupled in the visible spectrum and only two modes in the IR one. Despite Free Spectral Range (FSR) analysis allows to identify the 1^{st} and the 2^{nd} radial modes as the coupled families in the IR range, the same analysis does not hold in the visible range. Indeed, even though periodic peaks associated to different radial families can be recognized they show very similar FSR and they cannot be identified within the experimental uncertainty. For this reason we focused our attention on the brightest order family in the visible, labeled by squares in Fig. 5(top), showing transmittance and Q up to 20% and 20000, respectively. The IR spectrum, on the

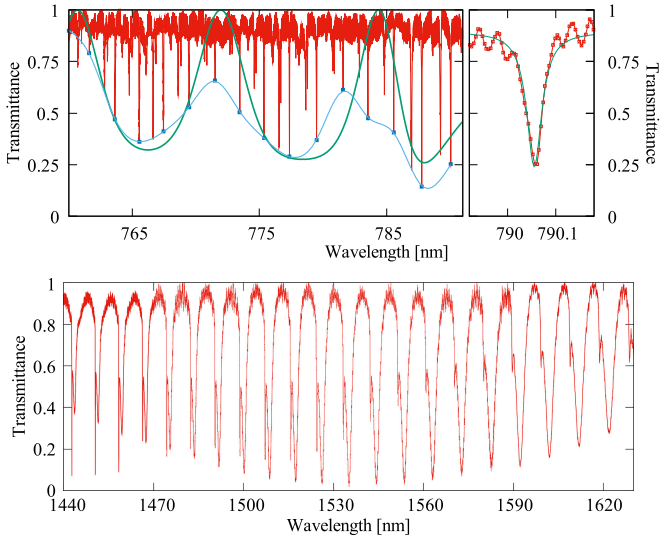

Fig. 5. (top-left) visible spectrum for wg_2 configuration; the transmittance minimum of the investigated family of resonances from the experiment (square symbols and interpolation line) is compared to the transmittance minimum obtained from the model (dashed line); (top-right) detail of an isolated resonance with a Lorentzian fit showing a resolution of 3 pm; (bottom) IR spectrum for wg_2 configuration with 1^{st} and 2^{nd} order family mode resonances.

TABLE I
FITTING PARAMETERS AS FOUND FOR FIG. 5 (TOP) AND FIG. 6

	$\Lambda[\mu\mathrm{m}]$	thickness [nm]	$\alpha[1/\mathrm{cm}]$	gap [nm]
vis	20 ± 10	100 ± 20	0.4 ± 0.1	670 ± 20
IR	12 ± 5	350 ± 50	0.6 ± 0.1	700 ± 50

other hand, is mainly characterized by complex resonance line shapes where the 2^{nd} order family modes ($Q \sim 1000$) are reactively coupled to the 1^{st} order family modes ($Q \sim 20000$) [18].

The two spectra constitute a first confirmation to the oscillatory model: the existence of peaks in the visible and IR spectra for the same device demonstrates that light over a 900 nm range can be coupled simultaneously to a resonator just by using the vertically coupled configuration. This feature cannot be explained by the point coupling models [9], [10], which allow only a single wavelength for the critical coupling condition (Fig. 3(bottom)).

Also the fine feature of the visible spectrum supports the model: oscillations of the resonance depth are present, resembling those of a directional coupler [14]. The oscillations are explained by the oscillatory coupling model as shown by the dashed line in Fig. 5. Simulation has been done by using the parameters reported in TABLE I. Even though the simulated curve does not fit perfectly the experimental one, a qualitative agreement can be observed, showing that the results derived from the model are consistent with the experiment.

A similar analysis on the transmittance cannot be performed for the IR spectrum, because the 1^{st} and the 2^{nd} order families strongly affects each other by a reactive coupling mechanism [18].

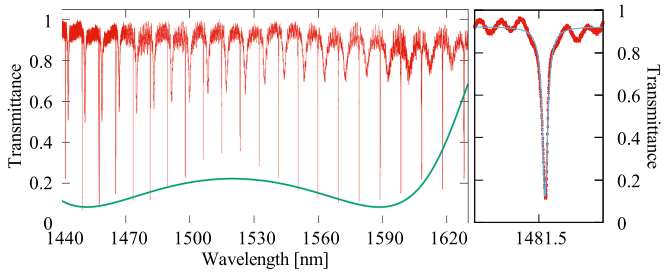

Fig. 6. (left) IR transmission spectrum of the wg_1 configuration and a fit of the model (line); (right) detail of an isolated resonance with Lorentzian fit showing a resolution of 1 pm.

However, by using the wg_1 configuration we are able to preferentially excite the first order radial family in the IR range (Fig. 6). In fact, when the waveguide is shifted 1 μm inside the resonator edge optimal overlap between the waveguide mode and the WGMr modes occurs for the first order radial mode [12]. With this wg_1 geometry, no signature of coupling in the visible is observed because the more confined visible modes do not overlap effectively with the bus waveguide mode.

Nonetheless, observation of the IR spectrum can still bring to a richer understanding of the physics of the system. The 1^{st} family in Fig. 6, well isolated from the 2^{nd} family, shows a peculiar shape describing a clear oscillation with a contrast of about 30%. An alternative possible explanation to this feature could rely on different material absorption channels (as for instance: Si-H bondings produced as residuals of the fabrication precess). However, the ellipsometry characterization revealed negligible material losses in this spectral region. As already pointed out, also the effect of a point coupling interaction cannot bring to such a behaviour, since the only oscillation that is expected from the model consists of a single dip in the transmittance. Actually, a reasonable explanation to this issue can be given by the oscillatory coupling model described above. Indeed, as found for the visible spectrum of wg_2, the transmittance minimum obtained from the model (line in Fig. 6) qualitatively follows the oscillating behavior of the experimental curve and, thus, confirms the oscillatory coupling model as a good description of vertically coupled systems. The parameters resulting from the fit in the two regimes are shown in Table I.

Despite the incertitude on the Λ values due to the approximations in the model, we notice that Λ and thickness are significantly different in the VIS and IR. In particular the thickness in the VIS range is not compatible with the experimental one ($\sim$350 nm). However, this apparent discrepancy can be solved by considering two peculiarities of the system: the geometry of the resonator and the coupling of higher order modes in the visible range. Indeed, the wedge shape of the resonator causes the thickness of the resonator in its external part to be strongly dependent on the radial position, starting from 350 nm at 21.5 μm radius and decreasing to 0 nm at 24 μm. In order to take this evidence into account in the model we consider the parameter thickness as an effective parameter, which corresponds to the resonator thickness felt by the optical modes along the coupling region. In addition to this, higher order modes in the visible range

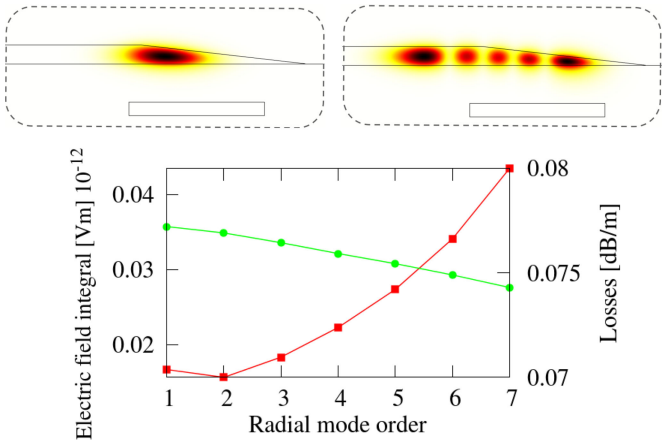

Fig. 7. (top panel) Mode profiles at $\lambda = 780$ nm for the 1^{st} order radial mode and for the 5^{th} order radial mode. (bottom panel) Integral of the electric field of the different resonator optical modes computed in the bus waveguide region (red line and squares) and propagation losses (green line and disk) for $\lambda = 780$ nm.

are pushed at larger radii by the wedge geometry (Fig. 7(top)) and they show a stronger electric field in the waveguide region (Fig. 7(bottom)) where the resonator effective height can be substantially lower than 350 nm. As a consequence to these considerations an effective thickness as low as 0.1 μm can be assumed in the visible range. The same geometrical argument (resonator optical modes propagating at larger radii) justifies the larger flat zone found for the visible modes with respect to the IR ones. Indeed, in the IR range only the 1^{st} and 2^{nd} order family of modes should be taken into account, since the higher order modes are absorbed by the Si substrate (see Appendix for details on substrate absorption). Losses and gap values are in agreement with values found in [13] and with Scanning Electron Microscope measurements respectively. At this point it is also worth to note that the developed model takes into account only first order modes for both the waveguide and the resonator, while higher order modes are present in the real structures at visible and IR wavelengths. These considerations can explain the difference between experimental data and simulated ones.

The curve presented in Fig. 6 shows that the model is not able to match perfectly the real system, yet. In particular, for long wavelengths the model predicts an increase in the transmittance which is not experimentally observed. For this reason, the use of full 3D simulations of the real system and the possibility to acquire data in different spectral regions (e.g. NIR) could constitute important thrusts for a more accurate modeling of the investigated device.

Other interesting information about the studied system can be extracted from a comparison of the Q of the 2^{nd} order family in the IR spectra for the wg_1 and wg_2 configurations. These are discussed in Appendix.

V. Conclusion

In this work we have experimentally demonstrated simultaneous coupling of visible and IR light in a WGM wedge resonator. The oscillatory coupling model, which describes this specific coupling geometry, has been extended to wavelength variations and a qualitative agreement with the experimental observations has been proven. Similarly, we have evidenced that the point coupling model fails in the description of vertically coupled structures. The large bandwidth achieved on a single resonator extends drastically the application possibilities and flexibility of an integrated device where the gap between the resonator and the bus waveguide is fixed. Indeed, it constitutes a desirable basis for the development of a multichannel technology [19] opening the possibility to further increase the number of operation per device. On the other hand, such scheme allows also to critically couple the various signals of a frequency conversion process resulting in an overall increase of the efficiency. Finally, the large bandwidth achieved on a single resonator must be added to other interesting features gained when vertical coupling is used, such as low cost CMOS compatible fabrication process, stable coupling with free-standing structures and wedge resonator coupling [12], [16], [20]. Consequently, it emerges that plenty of space is present for future development and employment of vertically coupled structure in the design of compact and cost-effective photonic chip.

Appendix
Quality Factor Analysis

A comparison of the 2^{nd} family resonances for the IR spectra in the two configurations can lead to a better understanding of the system. According to the transmittance values (see Fig. 5), in the wg_2 configuration, the system should change from under- to over-coupling regimes as the wavelength increases, fulfilling a critical coupling condition at about 1530 nm. Considering transmittance as the main information channel, wg_1 seems to follow the same behaviour, increasing its transmittance and thus becoming more and more overcoupled at higher wavelengths. Surprisingly, a similar analysis on the total Q returns different situation: the assumed overcoupled wg_1 configuration actually shows Q values always greater than those of wg_2, where the critical coupling condition is reached (see Fig. 8 top).

Despite the two analysis (on transmittance and on Q) seems to reach opposite results, a solution to this apparent inconsistency is obtained by considering the total losses (Γ_{tot}) composed by two main channels, the intrinsic one (Γ_{int}), due to the material, and the radiative one (Γ_{rad}), mainly due to coupling:

$$\Gamma_{\mathrm{tot}} = \Gamma_{\mathrm{int}} + \Gamma_{\mathrm{rad}} = \Gamma_{\mathrm{int}}(1+k) \tag{9}$$

where $k = \frac{\Gamma_{\mathrm{rad}}}{\Gamma_{\mathrm{int}}}$ is the coupling coefficient.

Then, the transmittance minimum value can be written as:

$$T_m = \left(\frac{\Gamma_{\mathrm{int}} - \Gamma_{\mathrm{rad}}}{\Gamma_{\mathrm{int}} + \Gamma_{\mathrm{rad}}}\right)^2 = \left(\frac{1-k}{1+k}\right)^2 \tag{10}$$

Experimental data of T_m extracted from the IR spectra have been used in Eq. (10) to obtain the two possible k solutions of this second order equation for both the configurations wg_1 and wg_2. Knowing that $\Gamma_{\mathrm{tot}} = \omega_0/Q_{\mathrm{tot}}$, Γ_{int} and Γ_{rad} values could be extracted from Eq. (9). Since Eq. (9) and Eq. (10) are symmetric for Γ_{rad} and Γ_{int} they can be swapped in the calculations with no variation on the results. Therefore unexpected behavior can be understood as follows. The

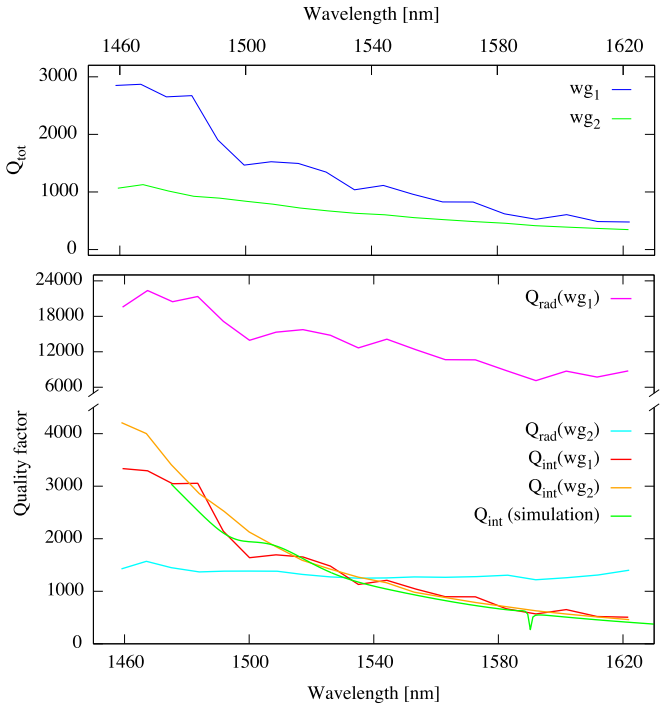

Fig. 8. (top) Quality factors from the IR spectra for wg_1 and wg_2; (bottom) Intrinsic and radiative quality factors for wg_1 and wg_2 configurations.

intrinsic Q (Q_{int}) are the same for both wg_1 and wg_2 showing a particular strong dependence on wavelength (see Fig. 8). The similarity of the two values is an expected result since the two resonators belong to the same processed wafer. In contrast to the 1^{st} family modes, showing oscillatory coupling (main text), the low confinement of the 2^{nd} one induces a remarkable coupling to the Si substrate of the wafer through the SiO_2 bottom cladding limiting the Q_{int} with a strong wavelength dependency. This assumption has been confirmed by a FEM simulation which perfectly match the experimental values (green line in Fig. 8). As expected, much lower losses are found for the wg_1 configuration, which becomes mainly dependent on intrinsic losses ($Q_t \approx Q_i$). In the wg_2 case the small difference between both loss channels (Γ_{rad} and Γ_{int}) results in an overall small Q, limited mainly by radiative losses for wavelengths below 1525 nm and by internal losses for higher wavelengths. In summary, the strong dependence of the intrinsic losses of the 2^{nd} family results in a peculiar behavior where the system remains in undercoupling regime in wg_1, whereas for wg_2 it passes from overcoupled to undercoupled when the wavelength is increased.

ACKNOWLEDGMENT

Authors M. Ghulinyan and G. Pucker would like to thank MNFLab-FBK staff for the support in realizing samples.

REFERENCES

[1] V. R. Almeida, C. A. Barrios, R. R. Panepucci, and M. Lipson, "All-optical control of light on a silicon chip," *Nature*, vol. 431, pp. 1081–1084, Aug. 2004.
[2] J. Ward, and O. Benson, "WGM resonator: Lasing, sensing and fundamental optics with microspheres," *Laser Photon. Rev.*, vol. 5, no. 4, pp. 553–570, 2011.
[3] A. Schliesser, and T. J. Kippenberg, "Cavity optomechanics with whispering-gallery mode optical micro-resonators," *Adv. Atomic, Mol. Opt. Phys.*, vol. 58, pp. 207–323, 2010.
[4] J. S. Levy, M. A. Foster, A. L. Gaeta, and M. Lipson, "Harmonic generation in silicon nitride ring resonators," *Opt. Express*, vol. 19, no. 12, pp. 11415–11421, 2011.
[5] A. Serpenguzel, S. Arnold, and G. Griffel, "Excitation of resonances of microspheres on an optical fiber," *Opt. Lett.*, vol. 20, no. 7 pp. 654–656, Apr. 1995.
[6] F. Treussart *et al.*, "Microlasers based on silica microspheres," *Ann. Telecommun.*, vol. 52, pp. 557–568, 1997.
[7] T. M. Benson, S. V. Boriskina, P. Sewell, A. Vukovic, S. C. Greedy, and A. I. Nosich, "Micro-optical resonators for microlasers and integrated optoelectronics," in *Frontiers in Planar Lightwave Circuit Technology*, vol. 216, Netherlands: Springer, 2006.
[8] A. B. Matsko, *Practical Application of Microresonators in Optics and Photonics*. New York, NY, USA: CRC Press, 2009.
[9] A. Yariv, "Critical coupling and its control in optical waveguide-ring resonator systems," *IEEE Photon. Technol. Lett.*, vol. 14, no. 4, pp. 483–485, Apr. 2002.
[10] S. M. Spillane, T. J. Kippenberg, O. J. Painter, and K. J. Vahala, "Ideality in a fiber-taper-coupled microresonator system for application to cavity quantum electrodynamics," *Phys. Rev. Lett*, vol. 91, no. 4, Jul. 2003, Art. no. 043902.
[11] T. Carmon, S. Y. T. Wang, E. P. Ostby, and K. J. Vahala, "Wavelength-independent coupler from fiber to an on-chip cavity, demonstrated over an 850 nm span," *Opt. Express*, vol. 15, no. 12, pp. 7677–7681, 2007.
[12] M. Ghulinyan, R. Guider, G. Pucker, and L. Pavesi, "Monolithic whispering-gallery mode resonators with vertically coupled integrated bus waveguides," *IEEE Photon. Technol. Lett.*, vol. 23, no. 16, pp. 1166–1168, Aug. 2011.
[13] M. Ghulinyan *et al.*, "Oscillatory vertical coupling between a whispering-gallery resonator and a bus waveguide," *Phys. Rev. Lett.*, vol. 110, no. 16, Apr. 2013, Art. no. 163901.
[14] B. E. Little, and W. P. Huang, "Coupled-mode-theory for optical waveguides," *Progress Electromagn. Res.*, vol. 10, pp. 217–270, 1995.
[15] B. E. A. Saleh, and M. C. Teich, *Fundamentals of Photonics*, Hoboken, NJ, USA: Wiley, 2007.
[16] F. Ramiro-Manzano, N. Prtljaga, L. Pavesi, G. Pucker, and M. Ghulinyan, "A fully integrated high-Q whispering gallery wedge resonator," *Opt. Express*, vol. 20, no. 20, pp. 22934–22942, Sep. 2012.
[17] D. Gandolfi, F. Ramiro-Manzano, F. J. Aparicio Rebollo, M. Ghulinyan, G. Pucker, and L. Pavesi, "Role of edge inclination in an optical microdisk resonator for label-free sensing," *Sensors*, vol. 15, no. 3, pp. 4796–4809, Feb. 2015.
[18] M. Ghulinyan *et al.*, "Intermode reactive coupling induced by resonator-waveguide interaction," *Phys. Rev. A*, vol. 90, no. 5, Nov. 2014, Art. no. 053811.
[19] L-W. Luo *et al.*, "High bandwidth on-chip silicon photonic interleaver," *Opt. Express*, vol. 18, no. 22, pp. 23079–23087, Oct. 2010.
[20] F. Ramiro-Manzano, N. Prtljaga, L. Pavesi, G. Pucker, and M. Ghulinyan, "Monolithic integration of High-Q wedge resonators with vertically coupled waveguides," *Proc. SPIE*, vol. 8767, May. 2013, Art. no. 876704.

Authors' biographies not available at the time of publication.